HAL
open science

The heterogeneous chemical kinetics of N2O5 on CaCO3 and other atmospheric mineral dust surrogates

F. Karagulian, C. Santschi, M. J. Rossi

To cite this version:

F. Karagulian, C. Santschi, M. J. Rossi. The heterogeneous chemical kinetics of N2O5 on CaCO3 and other atmospheric mineral dust surrogates. Atmospheric Chemistry and Physics, 2006, 6 (5), pp.1373-1388. hal-00295889

HAL Id: hal-00295889

https://hal.science/hal-00295889v1

Submitted on 18 Jun 2008

HAL is a multi-disciplinary open access archive for the deposit and dissemination of scientific research documents, whether they are published or not. The documents may come from teaching and research institutions in France or abroad, or from public or private research centers.

L'archive ouverte pluridisciplinaire **HAL**, est destinée au dépôt et à la diffusion de documents scientifiques de niveau recherche, publiés ou non, émanant des établissements d'enseignement et de recherche français ou étrangers, des laboratoires publics ou privés.

Atmos. Chem. Phys., 6, 1373–1388, 2006
www.atmos-chem-phys.net/6/1373/2006/
© Author(s) 2006. This work is licensed
under a Creative Commons License.

Atmospheric Chemistry and Physics

The heterogeneous chemical kinetics of N_2O_5 on $CaCO_3$ and other atmospheric mineral dust surrogates

F. Karagulian, C. Santschi, and M. J. Rossi

Ecole Polytechnique Fédérale de Lausanne(EPFL), Laboratoire de Pollution Atmosphérique et Sol (LPAS), Bâtiment CH H5, Station 6, CH-1015 Lausanne, Switzerland

Received: 7 September 2005 – Published in Atmos. Chem. Phys. Discuss.: 24 October 2005
Revised: 6 February 2006 – Accepted: 28 February 2006 – Published: 2 May 2006

Abstract. Uptake experiments of N_2O_5 on several mineral dust powder samples were carried out under continuous molecular flow conditions at 298±2 K. At $[N_2O_5]_0$=(4.0±1.0)×10^{11} cm^{-3} we have found γ_{ss} values ranging from (3.5±1.1)×10^{-2} for $CaCO_3$ to (0.20±0.05) for Saharan Dust with γ_{ss} decreasing as $[N_2O_5]_0$ increased. The uptake coefficients reported in this work are to be regarded as upper limiting values owing to the fact that they are based on the geometric (projected) surface area of the mineral dust sample. We have observed delayed production of HNO_3 upon uptake of N_2O_5 for every investigated sample owing to hydrolysis of N_2O_5 with surface-adsorbed H_2O. Arizona Test Dust and Kaolinite turned out to be the samples that generated the largest amount of gas phase HNO_3 with respect to N_2O_5 taken up. In contrast, the yield of HNO_3 for Saharan Dust and $CaCO_3$ is lower. On $CaCO_3$ the disappearance of N_2O_5 was also accompanied by the formation of CO_2. For $CaCO_3$ sample masses ranging from 0.33 to 2.0 g, the yield of CO_2 was approximately 42–50% with respect to the total number of N_2O_5 molecules taken up. The reaction of N_2O_5 with mineral dust and the subsequent production of gas phase HNO_3 lead to a decrease in $[NO_x]$ which may have a significant effect on global ozone.

1 Introduction

Dinitrogen pentoxide, N_2O_5, is part of the family of active nitrogen, NO_y, owing to its equilibrium with NO_2 and NO_3 according to Reaction (R1):

$$N_2O_5 \leftrightarrows NO_2 + NO_3 \quad \text{(R1)}$$

Under atmospheric pressure and 298 K the thermal lifetime of N_2O_5 is approximately 20 s and is a strong function of temperature (Atkinson et al., 1997; Wängberg et al., 1997). The observation of the buildup of the concentration of nitric acid, HNO_3, in the polluted urban planetary boundary layer (PBL) during the night could only be explained by the heterogeneous conversion of N_2O_5 to HNO_3 according to Reaction (R2) (Hjorth et al., 1987; Tuazon et al., 1983).

$$N_2O_5 + H_2O_{(ads)} \rightarrow 2HNO_3 \quad \text{(R2)}$$

The substrate for the heterogeneous Reaction (R2) has not been unambiguously identified but is thought to be urban H_2O-containing aerosols or humid surfaces on the ground whose purpose is to make available adsorbed H_2O in order to enable Reaction (R2).

Together with HNO_3 and NO_3, N_2O_5 contributes to the formation of particulate nitrate on the dust particles by surface processes in the troposphere (Zhang et al., 1994). These heterogeneous processes represent an important sink for nitrogen oxide species, with decreases of daytime NO_y levels reaching up to 60% in the presence of dust at a loading of about 1.8–11.5 $\mu g\,m^{-3}$ corresponding to a particle surface area of (0.11–0.7)×10^{-6} $cm^2\,cm^{-3}$. During the nighttime, the conversion of NO_3 and N_2O_5 to particles dominates the overall nitrate formation accounting for 80% of total particulate nitrate formation while the heterogeneous hydrolysis pathway leading to HNO_3 accounts for only about 20% (Zhang et al., 1994).

In addition, the present study shows that gas phase HNO_3 is a potential reaction product formed by heterogeneous hydrolysis of N_2O_5 with adsorbed water present on mineral dust. Previous laboratory studies performed using a Knudsen cell flow reactor have extensively supported the reactivity of HNO_3 on $CaCO_3$, marble, mineral dust surrogates and metal oxides (Fenter et al., 1995; Frinak et al., 2004; Hanisch and Crowley, 2001a; Underwood et al., 2001).

Mineral aerosols provide reactive surfaces in the atmosphere where heterogeneous chemical reactions may take place. Dentener showed that the interaction of N_2O_5, O_3 and

Correspondence to: M. J. Rossi
(michel.rossi@epfl.ch)

Table 1. Characteristic parameters and relevant kinetic expressions.

Definition	Value
Reactor volume, V	2000 cm^3
Reactor surface area, A_r	1500 cm^3
Sample surface area, A_s	19.5 cm^2 (TEFLON holder), 4.5 cm^2 (DELRIN holder)
Collision frequency ω for N_2O_5 with A_s (M=108)	ω=1.81$(T/M)^{1/2}A_s$
Orifice diameters (nominal)	1, 4, 8 and 14 mm
Rate constant of effusion	$k_{esc}(s^{-1})$
k_{esc} (Experimentally determined values for orifice diameters of nominal diameter)	0.02$(T/M)^{1/2}$ s^{-1} for 1 mm orifice 0.25$(T/M)^{1/2}$ s^{-1} for 4 mm orifice 0.8$(T/M)^{1/2}$ s^{-1} for 8 mm orifice 1.9$(T/M)^{1/2}$ s^{-1} for 14 mm orifice
Observed rate constant for heterogeneous reaction from steady state experiments, S_i=initial MS-signal; S_f=final MS-signal	$k_{obs}=(S_i/S_f-1)k_{esc}$
Measured uptake coefficient	$\gamma_{obs}=k_{obs}/\omega$

HO_2 radicals with dust will affect the photochemical oxidant cycle, with ozone concentrations decreasing by up to 10% in and nearby the dust source areas (Dentener et al., 1996).

Field observations (de Reus et al., 2005) and laboratory experiments (Hanisch and Crowley, 2001a, b, 2003c, d; Usher et al., 2003) have established the interaction of trace gases with mineral dust aerosol as well as the quantitative impact of the latter on the composition of the atmosphere. Box, regional and global scale models have shown the importance of dust on both the photochemical rates of oxidant formation as well as the loss of trace gases regarding atmospheric composition (Bauer et al., 2004; Bian and Zender, 2003; Dentener et al., 1996; Tabazadeh et al., 1998; Zhang et al., 1994). In these models the chemical alteration of the troposphere by dust including photolysis rate forcing and uptake was investigated. These models simulate the uptake of reactive trace gases on mineral dust surfaces in a global circulation model that includes schemes to simulate atmospheric chemistry processes in the presence of dust aerosol, sometimes using estimated rate coefficients for trace gas uptake.

The comparison of the global scale model of Bian and Zender with Bauer et al. reveals significant quantitative differences of the effect of mineral dust on O_3 and several important trace gases such as HNO_3, N_2O_5 and H_2O_2. However, both studies agree that the direct interaction of O_3 with mineral dust is of minor importance, whereas the uptake of one of its precursor, HNO_3, is responsible for most of the ozone decrease in the areas affected by dust. In the modelling studies of both Bian and Zender and Bauer et al. an uptake coefficient $\gamma_{N_2O_5}=10^{-3}$ at a relatively humidity (rh) of 30% has been used. In the modelling simulation performed by Bauer et al. the uptake of N_2O_5 resulted in a reduction of 11% of its concentration in the gas phase whereas the simulations of Bian and Zender indicate a global reduction of 2%.

Despite the published results of field observations and modeling studies (Bauer et al., 2004; Bian and Zender, 2003; Bonasoni et al., 2004; de Reus et al., 2000), only a single laboratory study has been performed on N_2O_5 interacting with Saharan Dust combining a Knudsen flow reactor with a DRIFTS cell (Seisel et al., 2005). We have therefore embarked on a laboratory program to measure some of the heterogeneous reactions involving N_2O_5 and NO_3 (Karagulian and Rossi, 2005) as relevant trace atmospheric gases. In the present work, we have used a Knudsen flow reactor in order to investigate the uptake and reaction of N_2O_5 on selected authentic mineral dust samples such as Kaolinite, Saharan Dust from Cape Verde Islands, Arizona test dust and natural limestone as well as on samples of pure $CaCO_3$.

2 Experimental set up and detection

All experiments were performed in a TEFLON® coated Knudsen flow reactor operating in the molecular flow regime. This technique has been described in detail in the literature (Caloz et al., 1997). Briefly, N_2O_5 was introduced into the Knudsen flow reactor from the gas handling system using a fine needle valve as a flow control device. An isolation plunger allows the separation of the reactive surface of interest from the reactor volume. The gases leave the Knudsen reactor through an escape orifice whose diameters (1, 4, 8, 14 mm) determine the residence time ($\tau_g=1/k_{esc}$) and molecular concentration at a given flow rate $F_0^M=I_M \cdot C_{(M)}$, where I_M is the mass spectrometric signal amplitude (MS) and $C_{(M)}$ is a calibration factor for the species M of interest that depends on instrumental parameters. The concentration $[M]_{MS}=N/V_{cell}=\frac{F_0^M}{k_{esc} \cdot V_{cell}}$ is related to the flow of molecules leaving the reactor F_0^M. Mass spectrometry (MS) provides a direct measure of the flow rate F_0^M which is proportional to

Table 2. Composition of mineral dust samples used in this work.

Kaolinite[1]	$CaCO_3$[2]	Natural limestone[3]	Saharan Dust[4]	Arizona Test Dust[5]
$Al_2Si_2O_5(OH)_4$	$CaCO_3$ 99.9%	$CaCO_3$ 97%	SiO_2 47%	SiO_2 68–76%
SiO_2 44.2%		SiO_2 1.9%	FeO 14.7%	Al_2O_3 10–15%
TiO_2 2.17%		$Al_2O_3$0.5%	Al_2O_3 17.6%	Fe_2O_3 2–5%
Al_2O_3 37.2%		Fe_2O_3 0.3%	MgO 5.1%	Na_2O 2–4%
Fe_2O_3 1.14%		MgO 0.2%	Na_2O 2.1%	CaO 2–5%
FeO 0.05%		Other elements 0.1%	K_2O 2.5%	MgO 1–2%
MgO 0.04%			CaO 5.0%	TiO_2 0.5–1.0%
CaO 0.04%			TiO_2 4.5%	K_2O 2–5%
Na_2O 0.02%			P_2O_5 0.6%	
K_2O 0.02%			SO_3 0.3%	
P_2O_5 0.06%			MnO 0.3%	
F 0.02%				
ρ_t=2.1–2.6 g/cm^3	ρ_t=2.93 g/cm^3	ρ_t=2.7 g/cm^3	ρ_t=2.7 g/cm^3	ρ_t=2.65 g/cm^3
ρ_b=0.528 g/cm^3	ρ_b=0.96 g/cm^3	ρ_b=1.13 g/cm^3	ρ_b=1.2 g/cm^3	ρ_b=0.6 g/cm^3
d=1.0 μm	d=3.5 μm	–	d=0.9 μm	–
S_{BET}=22.57 m^2/g	S_{BET}=5.06 m^2/g	–	S_{BET}=39.6 m^2/g	–

[1] C. V. Clemency, Dept. of Geological Sciences, SUNY at Buffalo, Buffalo N. Y. (USA), for the Clay Minerals Society.
[2] Fluka AG, CH-9471 Buchs (Switzerland).
[3] Transmat SA, Route de Ferreyres, CH-1315 La Sarraz (Switzerland).
[4] Hanisch F. and Crowley, J. N. Atmos. Chem. Phys., 3, 119, 2003.
[5] Powder Technology Inc., 1433 Ewing Avenue S. Burnsville, MN 55 306, USA.

the concentration of a species escaping the Knudsen flow reactor. The rate constant for the effusive loss k_{esc} of N_2O_5 is given by the kinetic theory of gases and was measured for every used orifice. The characteristic parameters and relevant kinetic expressions used in this work are reported in Table 1.

The samples we have used in this study are the following: Kaolinite, poorly ordered (KGa-2, Warren County, Georgia, USA), $CaCO_3$ (Fluka), Arizona Medium Test Dust (Powder Technology Incorporated, Burnsville MN, USA), natural limestone (Transmat, La Sarraz, Switzerland) and Saharan Dust from deposits on Cape Verde Islands (SDCV). The main physical and chemical data on the mineral dust samples used in this work are reported in Table 2.

Two kinds of sample holders were used: one consisted of a TEFLON coated Pyrex holder of available sample surface of 19.6 cm^2, the other consisted of an internal reduction piece made out of DELRIN leading to a sample surface of 4.9 cm^2. Both TEFLON and DELRIN did not show any reactivity towards N_2O_5 under the present experimental conditions.

N_2O_5 was synthesized by the oxidation of NO_2 with excess ozone. MS analysis did not reveal the presence of ozone at m/e 48. The O_3/O_2 mixture at the outlet of the ozonator (Fisher 502) is passed through a P_2O_5 trap in order to eliminate residual moisture before being mixed with equally dried NO_2. The N_2O_5 is collected in a methanol/dry-ice bath at 195 K and is subsequently analyzed for purity by MS. Hydrolysis of N_2O_5 may occur on surfaces of the traps and of the vacuum line before admission into the Knudsen flow reactor generating HNO_3 as an impurity ranging from 10 to 15% as detected by MS at m/e 63, its molecular ion peak.

N_2O_5 does not have a measurable parent and fragment peak at m/e 108 and 62, respectively, under the present experimental conditions; the most intense peaks are its fragment NO_2^+ at m/e 46 followed by the less intense fragment NO^+ at m/e 30. However, the HNO_3 impurity also contributes to the MS signal at m/e 46 and 30. Under the used experimental conditions, HNO_3 has been detected at its parent peak at m/e 63. Through a calibrated mass spectrum of pure HNO_3 we have accurately determined the effective contribution of HNO_3 at m/e 46 and 30 by using the fragmentation pattern expressed as the ratios $f_{46}=\frac{I_0^{46(HNO)_3}}{I_0^{63(HNO)_3}}=52\pm8$ and $f_{30}=\frac{I_0^{30(HNO)_3}}{I_0^{63(HNO)_3}}=33\pm4$. In the absence of a substrate, $f_{46}\cdot I_0^{63(HNO_3)}$ and $f_{30}\cdot I_0^{63(HNO_3)}$ have been subtracted from the total MS signals I_0^{46} and I_0^{30} at m/e 46 and 30, respectively, in order to assign the remaining MS amplitude to the NO_2^+ and NO^+ fragments of N_2O_5: $I_0^{46(N_2O_5)}=I_0^{46}-f_{46}\cdot I_0^{63(HNO_3)}$ and $I_0^{30(N_2O_5)}=I_0^{30}-f_{30}\cdot I_0^{63(HNO_3)}$. The ratio between the two most intense peaks of N_2O_5 therefore was $r=\frac{I_0^{46(N_2O_5)}}{I_0^{30(N_2O_5)}}=1.4\pm0.2$. Mixtures of N_2O_5 and HNO_3 may thus be monitored using MS signal intensities at m/e 46, 30 and 63. However, in order to quantify N_2O_5 we chose its most intense peak corresponding to its fragment NO_2^+ at m/e 46. Naturally, the

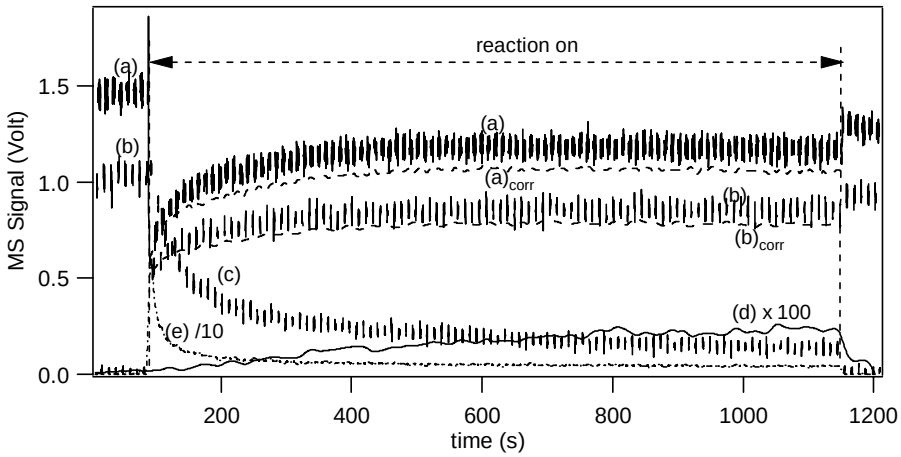

Fig. 1. Typical N_2O_5 uptake experiment on a sample of 510 mg of $CaCO_3$. Curves (a), (b), (c), (d) and (e) correspond to the raw MS signals monitored at m/e 46, m/e 30, m/e 44, m/e 63 and m/e 18, respectively, using an orifice diameter of 14 mm, A_s=19.6 cm^2 and $[N_2O_5]_0$=(4.0±1.0)×10^{11} cm^{-3}. Curves $(a)_{corr}$ and $(b)_{corr}$ correspond to the corrected signal at m/e 46 and m/e 30 for the presence of HNO_3.

MS fragment m/e 46 was corrected for the contribution of HNO_3 in order to calculate $[N_2O_5]$. The subscript 0 and r refers to continuous gas uptake experiments in the absence and presence, respectively, of the solid sample.

3 Uptake coefficient of N_2O_5 and identify of reaction products

When N_2O_5 is exposed to the sample, it is taken up and undergoes a heterogeneous reaction on the mineral dust surface which results in a decrease of the N_2O_5 concentration that is monitored using the MS signal $I_r^{46(N_2O_5)}$. As shown in previous studies on mineral dust, HNO_3 that is always present as an impurity, is taken up on the mineral dust surface without releasing any product that may contribute to the total MS signal I_r^{46} at m/e 46 (Hanisch and Crowley, 2001b). We have therefore determined the rate constant k_{obs} for the disappearance of N_2O_5 following Eq. (1), assuming that the rate law is first order in N_2O_5:

$$k_{obs} = \frac{I_0^{46(N_2O_5)}}{I_r^{46(N_2O_5)}} - 1 \cdot k_{esc} \quad (1)$$

$I_0^{46(N_2O_5)}$ and $I_r^{46(N_2O_5)}$ are the intensities of the NO_2^+ fragment of N_2O_5 before and during heterogeneous reaction, respectively, and k_{esc} is the measured rate constant of effusion for N_2O_5 out of the flow reactor (see Table 1). In order to determine $I_r^{46(N_2O_5)}$, the raw MS signal at m/e 46 was corrected for HNO_3 generated through hydrolysis of N_2O_5 with water adsorbed on the substrate surface. Production of HNO_3 has in fact been observed at m/e 63 in every uptake experiment of N_2O_5. Figure 1 shows the raw MS signal at m/e 63 for a typical uptake experiment of N_2O_5 on $CaCO_3$. Therefore, we have corrected the MS signal of N_2O_5 at m/e 46 for the presence of HNO_3 according to Eq. (2) when the sample is exposed to N_2O_5:

$$I_r^{46(N_2O_5)} = I_r^{46} - f_{46} \cdot I_r^{63(HNO_3)} \quad (2)$$

The ratio r, reported above, turned out to be the same before and during the exposure of the mineral dust sample to N_2O_5. Therefore, $I_r^{46(N_2O_5)}$ exclusively corresponds to N_2O_5 for this experiment after correction of the MS signal at m/e 46 for the contribution of HNO_3 desorbing from the mineral dust substrate.

In the Knudsen flow reactor, reactant gas molecules either exit through an aperture into the mass spectrometer or are lost on the reactive surface. The net observed uptake coefficient for N_2O_5, γ_{obs} is given by the following expression:

$$\gamma_{obs} = \frac{k_{obs}}{\omega} \quad (3)$$

Equation (3) is only valid if the rate law for uptake is first order in N_2O_5, where k_{obs} is the pseudo-first order rate constant at steady state conditions given in Eq. (1), ω is the collision frequency of the average molecule with the reactive surface area of the sample defined as $\omega = \frac{\bar{c}}{4V_{cell}} A_s$, $\bar{c}$ is the mean velocity of the gas-phase molecule, V_{cell} is the volume of the reactor and A_s is the surface sample area. In our data analysis, γ_{obs} was calculated using the geometric surface area of the sample holder as will be justified below. In the following, we evaluate γ_{obs} at the initial and steady state values of the uptake rate leading to γ_0 and γ_{ss}, respectively.

4 Uptake of N_2O_5 on $CaCO_3$: results and discussion

Typical raw data from an uptake experiment of N_2O_5 on 510 mg of $CaCO_3$ are shown in Fig. 1 using the 14 mm

Table 3. Uptake experiments with N_2O_5 on $CaCO_3$ as a function of sample mass at $[N_2O_5]_0$=(4.0±1.0)×10^{11} cm^{-3}.

$CaCO_3$ Mass in g	γ_0	γ_{ss}	Yield of HNO_3^c	Yield of CO_2^c
0.33[a]	0.16 ± 0.03	(2.0±0.6)×10^{-2}	5.2 %	47.8 %
0.51[a,b]	0.2 ± 0.05	(2.2±0.5)×10^{-2}	5.4 %	42.4 %
0.58[a]	0.18±0.05	(2.3±0.5)×10^{-2}	–	–
0.73[a]	0.22±0.04	(2.4±0.4)×10^{-2}	5.4 %	50 %
2[a]	0.18±0.025	(1.6±1.6)×10^{-2}	5.4 %	50 %

[a] Uptake measurements performed with a surface sample area A_s=19.6 cm^2.
[b] Uptake experiment displayed in Fig. 1.
[c] The yield is given as a percentage with respect to the total number of molecules of N_2O_5 taken up during a reaction time of 550 s.

diameter-orifice. After a steady state flow of N_2O_5 has been established, the isolation plunger is lifted at t=92 s and the substrate is thus exposed to the N_2O_5 flow. MS signals of 18 (H_2O^+), 30 (NO^+), 44 (CO_2^+), 46 (NO_2^+), and 63 (HNO_3^+) were simultaneously monitored during the uptake. Because of the uptake of N_2O_5 on $CaCO_3$, the number of molecules exiting through the escape orifice into the MS immediately decreases which leads to a decrease of the MS signal $I_r^{46(N_2O_5)}$ at m/e 46. During the exposure of the sample to N_2O_5 both HNO_3 and CO_2 monitored at m/e 63 and 44, respectively, have been observed in the gas phase. As the exposure time increases, the MS signal at m/e 46 partially recovers, indicating a decrease in the rate of uptake that ultimately leads to steady state towards the end of the displayed uptake experiment. However, on the time scale of an hour or longer the uptake begins to saturate at the present experimental conditions so that one should preferably talk about a pseudo steady-state that is attained at the end of the uptake experiment at t=1150 s displayed in Fig. 1. As a conclusion we note the disparate time scales for the partial saturation of N_2O_5 uptake taking place during the first 300 s and complete saturation occurring on a much longer time scale. At t=1150 s the sample compartment is sealed by lowering the plunger and the MS signal at m/e 46 approximately returns to its initial steady-state value. The slight decrease of $I_0^{46(N_2O_5)}$ over extended periods of time such as displayed in Fig. 1 is explained by a slight decrease of the corresponding flow rate into the reactor owing to the difficulty of maintaining a stable pure N_2O_5 flow for long exposure times.

An ancillary experiment was performed in order to estimate the amount of water adsorbed on the $CaCO_3$ substrate surface after a given pumping time. In order to limit H_2O desorbing from the Pyrex sample holder it was replaced by a gold-coated all-metal sample holder. In this way most desorbing H_2O may be attributed to the mineral dust sample. Typically, a fresh sample of 1g of $CaCO_3$ was pumped for 30 min at T=298 ± 2 K in the 14 mm-orifice reactor until the MS signal of H_2O at m/e 18 dropped to the background level. Subsequently, the $CaCO_3$ sample was heated up to 470 K and the MS signal at m/e 18 recorded until it reached background as well indicating that no additional water desorbed at that temperature. The MS signal at m/e 18 was integrated in order to calculate the number of adsorbed water molecules H_2O_{ads} using the measured BET surface area of 3.7 m^2 g^{-1} for a high ordered commercially available $CaCO_3$ sample from Aldrich Corporation. A value of approximately 3.0×10^{13} molecule cm^{-2} has been found for the surface density of strongly adsorbed H_2O_{ads} (Santschi, 2003).

When the $CaCO_3$ substrate is exposed to N_2O_5 at 92 s, we observed rapid formation of $CO_{2(g)}$ and $H_2O_{(g)}$ as displayed in Fig. 1 which were either generated in a chemical reaction or desorbing from a precursor state. In order to better understand the uptake of N_2O_5 on solid $CaCO_3$ powder, we will briefly digress to the description of the chemical nature of a carbonate surface. From experimental and theoretical surface science studies, (De Leeuw and Parker, 1998; Kuriyavar et al., 2000; Stipp et al., 1994) there is clear evidence that under ambient conditions of pressure, temperature, and relative humidity, the surface of $CaCO_3$ is terminated by OH groups that persist even under ultrahigh vacuum conditions. The OH-terminated surface may be a result of the dissociative adsorption of water according to Reaction (R3):

$$CaCO_3 + H_2O \rightarrow Ca(OH)(HCO_3) \quad \text{(R3)}$$

In a recent study (Al-Hosney and Grassian, 2004), the surface chemistry of $CaCO_3$ with trace atmospheric gases such as HNO_3, SO_2, HCOOH, and CH_3COOH was investigated using FTIR absorption spectrometry. This study has suggested adsorbed carbonic acid H_2CO_3 to be involved in the surface chemistry of $CaCO_3$ and was reportedly identified as a stable intermediate species on the $CaCO_3$ surface in the presence of H_2O vapor. The vibrational spectrum of carbonic acid is characterized by its C=O stretching frequency at 1685 and 1705 cm^{-1} corresponding to the adsorbed and condensed phase, respectively. In the following, adsorbed H_2CO_3 will occur as an intermediate in several instances.

Dissolution of $CaCO_3$ in the system $H_2O - CO_2 - CaCO_3$ is controlled by three molecular processes: dissolution at the mineral surface, mass transport by diffusion, and the slow Reaction (R4) which have been modelled by Buhmann and Dreybrodt (Buhmann and Dreybrodt, 1985) with Reaction (R4) being rate limiting (Dreybrodt et al., 1997):

$$CO_{2(g)} + H_2O_{(ads)} \leftrightarrows H_2CO_{3(ads)} \leftrightarrows H^+_{(aq)} + HCO^-_{3(aq)} \quad \text{(R4)}$$

Bicarbonate ion, HCO_3^-, may react with $CaCO_3$ to yield a surface intermediate that is proposed to be the active surface reactant for the heterogeneous reactions discussed below according to the well-known "Karst dissolution" mechanism (Dreybrodt et al., 1996):

$$CaCO_{3(s)} + H^+_{(ads)} + HCO^-_{3(ads)} \rightarrow Ca(OH)(HCO_3) + CO_{2(g)} \quad \text{(R5)}$$

When the $CaCO_3$ sample is exposed to N_2O_5 the surface intermediate may react as follows:

$$N_2O_{5(g)} + Ca(OH)(HCO_3) \rightarrow Ca(NO_3)_2 + H_2O_{(s)} + CO_{2(g)} \quad \text{(R6)}$$

and the net reaction resulting from Reactions (R4), (R5) and (R6) will be:

$$N_2O_5 + CaCO_3 \rightarrow Ca(NO_3)_2 + CO_{2(g)} \quad \text{(R7)}$$

Reaction (R5) is much too slow under flow reactor conditions such that the surface intermediate $Ca(OH)(HCO_3)$ may only be formed under ambient conditions and at long reaction times according to a recent laboratory study (Santschi and Rossi, 2006). Once the surface intermediate is consumed, the surface reaction will saturate. Therefore, the rate and the extent of the heterogeneous reaction depend on the abundance of the preexisting surface intermediate. On the time scale of the uptake experiments reported in Fig. 1 the calculated ratio CO_2/N_2O_5 of the product yields was 0.42 which is significantly smaller than 1.0 that is stoichiometrically expected according to Reaction (R7) (see Table 3). The mass balance between the adsorbed N_2O_5 and the reaction product CO_2 is therefore not satisfied. If Reactions (R4) and (R5) were fast and not rate limiting, the expected CO_2 yield would be 100%. We therefore have to consider another possible pathway for Reaction (R6) that does not result in release of CO_2:

$$N_2O_5 + Ca(OH)(HCO_3) \rightarrow Ca(NO_3)(HCO_3) + HNO_{3(g)} \quad \text{(R8)}$$

In this case N_2O_5 may directly be converted into gas phase HNO_3 which is also observed at longer exposure times as displayed in Fig. 1. Reaction (R8) may therefore explain why the ratio CO_2/N_2O_5 is significantly smaller than 1.0 as no CO_2 is released from Reaction (R8). In addition, HNO_3 may also react with $CaCO_3$ as already observed by Hanisch and Crowley, 2001. We routinely measure a yield of 51% of gas phase H_2O with respect to N_2O_5 consumed which is comparable to the CO_2 yield according to Reaction (R6) and results from the uptake of N_2O_5 on samples of different mass of powdered $CaCO_3$. In the wake of the observation of H_2O, CO_2 and HNO_3 we propose that Reactions (R6) and (R8) compete with each other. H_2O is formed in Reaction (R6) on $CaCO_3$ whose reactive interface consists of the preexisting surface intermediate $Ca(OH)(HCO_3)$ resulting from prior exposure to atmospheric CO_2 and H_2O following Reactions (R4) and (R5).

In the present study we have mostly used a low-ordered commercially available $CaCO_3$ sample from Fluka Corporation. Owing to the fact that this $CaCO_3$ sample has a specific surface area (BET) of $5.06\,m^2/g$, the 510 mg sample from the experiment displayed in Fig. 1 has a total surface area of $2.6\times10^4\,cm^2$. N_2O_5 may be represented as a sphere with a projected surface area of $6.4\times10^{-15}\,cm^2$/molecule or 1.56×10^{14}/molecules cm^{-2}, assuming that N_2O_5 has a characteristic diameter of approximately 9 Å and a density of $2.93\,g/cm^3$. After an exposure time of 1060 s 2.2×10^{18} molecules of N_2O_5 are taken up on 510 mg of $CaCO_3$(Fig. 1) leading to a surface concentration of $\frac{2.2\times10^{18}}{2.6\times10^4}$=$8.4\times10^{13}N_2O_5$ molecule cm^{-2} which corresponds to a coverage (θ) of approximately 54% based on the BET surface area after a reaction time of 1060 s. After N_2O_5 reacted on $CaCO_3$ powder for 1060 s the substrate is apparently at steady state as displayed in Fig. 1. This means that there is a sufficient number of intermediate species $Ca(OH)(HCO_3)$ to allow Reactions (R6) and (R8) to occur. However, once reacted with N_2O_5, the intermediate species cannot regenerate because Reactions (R4) and (R5) are too slow. Therefore, we observe an amount of $CO_{2(g)}$ smaller than the maximum yield of 100% at steady state conditions. On the other hand, N_2O_5 may react with adsorbed water $H_2O_{(ads)}$that still remains on the $CaCO_3$ substrate, thereby forming two molecules of nitric acid as follows:

$$N_2O_{5(g)} + H_2O_{(ads)} \rightarrow 2HNO_{3(g)} \quad \text{(R9)}$$

In this case solid $CaCO_3$ is just the support for the reactive adsorbed water $H_2O_{(ads)}$ and is not consumed in the chemical reaction. Initially, $HNO_{3(g)}$ is physically adsorbed on the surface to result in adsorbed HNO_3 which reacts with a surface OH-group and slowly forms surface nitrates and H_2O according to Reaction (R10):

$$S{-}OH + HNO_{3(ads)} \rightarrow S{-}NO_3 + H_2O_{(ads,g)} \quad \text{(R10)}$$

where S represents a surface site for physical adsorption. This mechanism has been proposed by Seisel and co-workers (Seisel et al., 2004) in a DRIFTS study of the heterogeneous reaction of HNO_3 on mineral dust where they observed the presence of free OH-groups located on the surface of mineral dust and the formation of surface nitrates. The fact that CO_2 is formed immediately after lifting the plunger (Fig. 1) whereas HNO_3 is formed later on after a certain delay clearly indicates that there are two competitive processes occurring during the reaction of N_2O_5 with $CaCO_3$. Immediately after the exposure of substrate, N_2O_5 reacts with the intermediate species $Ca(OH)(HCO_3)$ on the $CaCO_3$ sample (Reactions R6

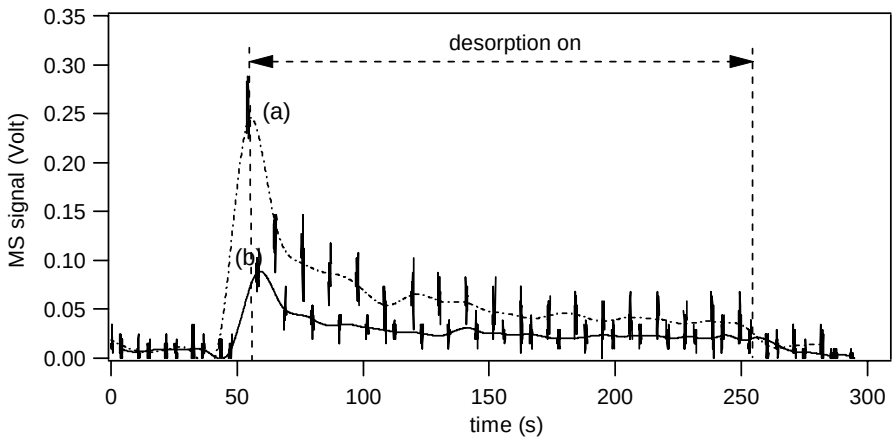

Fig. 2. Desorption of CO_2 and NO after N_2O_5 uptake on a sample of 510 mg $CaCO_3$ displayed in Fig. 1. Curves (a) and (b) correspond to the raw MS signals monitored at m/e 44 and m/e 30, respectively, at an orifice diameter of 14 mm and A_s=19.6 cm^2.

Table 4. Relationship between γ_0 and γ_{ss} at different residence times $\tau_g(s^{-1})$ of N_2O_5 interacting with 580 mg of $CaCO_3$ powder for data plotted in Fig. 2, surface sample area A_s=19.6 cm^2; $F_0^{N_2O_5}=2.3\times10^{15}$ molecule s^{-1}.

Orifice (mm)	γ_0	γ_{ss}	τ_g(s)
14	$(1.6\pm0.13)\times10^{-1}$	$(6.0\pm1.2)\times10^{-2}$	0.34
8	$(8.5\pm0.8)\times10^{-2}$	$(3.0\pm0.7)\times10^{-2}$	0.81
4	$(3.4\pm1.0)\times10^{-2}$	$(1.8\pm1.1)\times10^{-2}$	2.72
1	$(1.1\pm1.0)\times10^{-2}$	$(1.0\pm1.0)\times10^{-2}$	30

and R8). At the same time heterogeneous hydrolysis of N_2O_5 may occur due to the presence of $H_2O_{(ads)}$ on the substrate (Reaction R9). However, the presence of a sufficient quantity of the intermediate formed in Reaction (R5) may make Reactions (R6) and (R8) predominant at first with respect to Reaction (R9). This explains the initial rapid formation of $CO_{2(g)}$ and the absence of any measurable trace of gas phase HNO_3 at t=92 s in Fig. 1. Reaction (R6) may explain the slow rise of HNO_3 with the extent of reaction as $H_2O_{(ads)}$ is accumulating on the surface and increasingly enabling the heterogeneous hydrolysis of N_2O_5 according to Reaction (R9). Once the surface intermediate starts to be significantly depleted owing to the initial fast reaction with N_2O_5 Reactions (R6) and (R8) start saturating and Reaction (R9) becomes predominant which would explain the delayed formation of HNO_3 displayed in Fig. 1. At present we do not have sufficient data to identify the elementary processes, Reactions (R6), (R8) and (R9) with the partial saturation of N_2O_5 uptake during the initial 300 s of exposure as discussed above and displayed in Fig. 1. However, we expect the changing branching ratio between Reactions (R6) and (R8) on the one hand and the hydrolysis Reaction (R9) on the other hand with the extent of N_2O_5 uptake to play a significant role. This may well be a starting point for numerical modeling of the present reaction system.

After having performed the uptake experiment shown in Fig. 1 on a substrate of $CaCO_3$, we sealed the sample and halted the inlet flow of N_2O_5 for approximately 10 min. Subsequently, we lifted the plunger again and observed small amounts of desorbing CO_2 (curve (a), Fig. 2) as well as a MS signal at m/e 30 without any measurable MS signal at m/e 46 (curve (b), Fig. 2). The total yield of desorbed CO_2 only represented 5% of N_2O_5 taken up on the substrate of $CaCO_3$ during the reaction time of 1058 s (Fig. 1). The small intensity of the MS signal at m/e 30 suggests formation of small amounts of NO as a decomposition product of N_2O_5 owing to the absence of a MS signal at m/e 46.

Uptake experiments of N_2O_5 on 0.58 g of $CaCO_3$ powder were carried out at smaller orifice sizes, thus increased residence time τ_g at constant flow of N_2O_5 of 2.3×10^{15} molecule s^{-1}. The values of γ_0 and γ_{ss} decrease with increasing values of the residence time as displayed in Fig. 3 and Table 4. The strong dependence of γ_{ss} on τ_g suggests that the mechanism of N_2O_5 uptake is complex and does not correspond to a simple first order uptake reaction. These observations indicate that the reactivity of N_2O_5 on $CaCO_3$ decreases for long residence times as the heterogeneous reaction rate not only depends on the gas phase concentration but apparently also on intermediates whose surface concentration depend on the extent of reaction that scales with τ_g akin to an effective second order reaction. Apparently, the active surface intermediate $Ca(OH)(HCO_3)$ cannot regenerate under the present experimental conditions according to Reaction (R5). This is consistent with the preexisting nature of the surface intermediate discussed above.

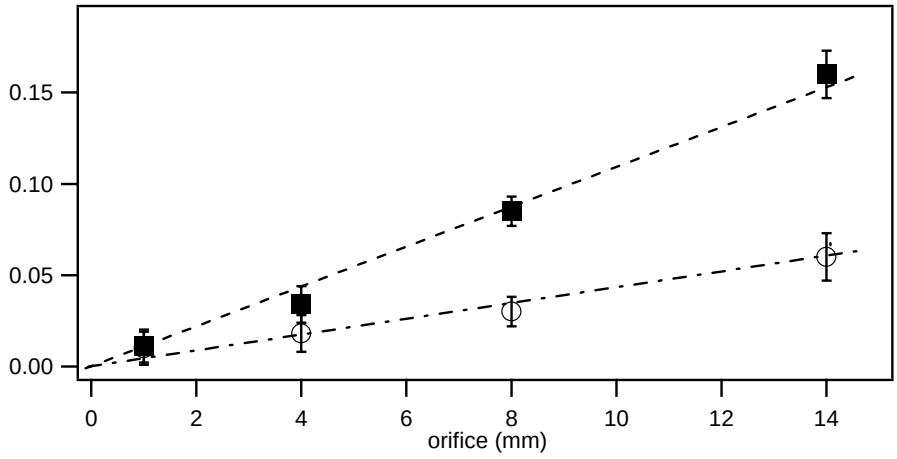

Fig. 3. Dependence of γ_0 (full squares) and γ_{ss} (open circles) for the uptake of N_2O_5 on 580 mg $CaCO_3$ powder on orifice size: A_s is 4.9 cm^2, $F_0^{N_2O_5}$=2.3×10^{15} molecule s^{-1}.

In order to unravel whether or not the effective available surface area for uptake is influenced by the internal surface area formed by interstitial voids between individual dust particles, the mass dependence of the N_2O_5 uptake on $CaCO_3$ was investigated in the Knudsen flow reactor at ambient temperature and at $[N_2O_5]$=(4.0±1.0)×10^{11} cm^{-3}. The mass of $CaCO_3$ which is a non-porous material ranged from 0.11 g to 1.8 g and the results are shown in Fig. 4. Table 5 reports values of γ_{ss} and γ_0 based on the geometric surface area A_s=19.6 cm^2. The steady state and initial uptake coefficient γ_{ss} and γ_0, respectively, of N_2O_5 were found to increase linearly with the mass of the $CaCO_3$ sample at low masses. Samples below 0.33 g were considered to be part of this linear mass-dependent regime. Increasing the sample mass further had a negligible effect on the amount of adsorbed N_2O_5 as apparently not the entire external sample surface is available for N_2O_5 adsorption. This maximum value is attributed to the inability of N_2O_5 to penetrate through all layers of the sample within the residence time of N_2O_5 in the gas phase, thus resulting in a constant number of molecules taken up despite the increasing sample mass. The limiting γ_{ss} value therefore represents the maximum amount of N_2O_5 able to interact with $CaCO_3$ powder within the N_2O_5 residence time.

The Reaction of N_2O_5 on $CaCO_3$ and other mineral dust substrates is significantly different to that observed in laboratory work on N_2O_5 on salt where it was concluded that N_2O_5 is non-sticky (Koch et al., 1999) and therefore able to penetrate into the interstitial voids of the alkali salt sample in contrast to mineral dust, presumably because of the difference in the number and types of surface OH-groups that seem to be more prevalent on mineral dust compared to alkali salts. We attribute a large value to γ for N_2O_5 on $CaCO_3$ because of the large initial uptake value γ_0 value reported in Table 6 at the low value of $[N_2O_5]$ of 4.0×10^{-11} cm^{-3} (γ_0=0.12 for $CaCO_3$) which effectively prevents the application of pore diffusion theory because reaction is much faster than Knudsen diffusion into the bulk. In view of the small atmospheric concentration of N_2O_5 of typically 5.0×10^9 cm^{-3} which is roughly two orders of magnitude lower than the lowest concentration used in the present experiments and the observed inverse concentration dependence of both γ_0 and γ_{ss} (Table 6, except for Kaolinite, see Fig. 8) the rate of uptake under atmospheric conditions will correspond to γ 0.12 such that we feel entitled to take the external surface as a basis to extract the γ values from the measured rates. In view of the low atmospheric $[N_2O_5]$ we confer more weight to γ_0 because it is mostly free of saturation effects that lower γ_0 to γ_{ss} values under the chosen experimental conditions as displayed in Fig. 1. Because we cannot attain concentration values of $[N_2O_5]$=5.0×10^9 cm^{-3} in the present experiment we simply attribute more weight to γ_0 than to γ_{ss} in that we believe that γ_0 more accurately describes the atmospheric value in view of the inverse concentration dependence.

In order to better define the saturation behavior of N_2O_5 on the substrate further uptake experiments were performed on $CaCO_3$ employing a pulsed valve to admit N_2O_5 into the reactor. The pulsed-valve experiments were carried out by using a solenoid valve, through which the gas was introduced in pulses with a duration of 5 ms and at a dose of 2.5×10^{15} molecules per pulse (Caloz et al., 1997) corresponding to $[N_2O_5]_0$=1.3×0^{12} cm^{-3}. We determined the total number of injected molecules per pulse and the value of k_{esc} in a reference experiment which was obtained by fitting the decaying MS signal to a single exponential decay in the absence of reaction thereby obtaining k_{esc}. The "reactive pulse" was obtained by repeating the same pulsed experiment with the sample exposed to the gas. The total observed exponential decay in the presence of a reactive substrate was thus

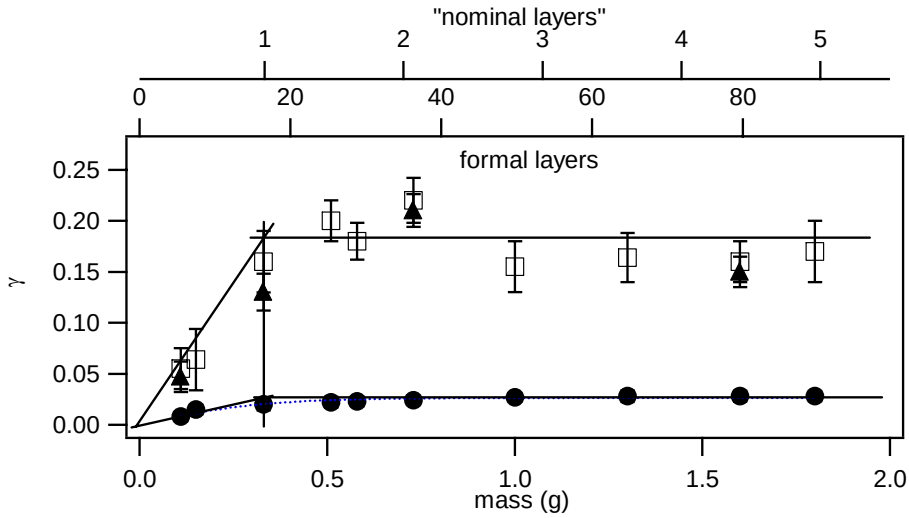

Fig. 4. Dependence of the uptake coefficient γ_0 (open squares) and γ_{ss}(full circles) on sample mass at $[N_2O_5]_0$=(4.0 ± 1.0)×10^{11} cm^{-3} at an orifice diameter of 14 mm for the uptake of N_2O_5 on $CaCO_3$ powder (A_s=19.6 cm^2). Full triangles represent pulsed valve experiments carried out at the same experimental conditions.

characterized by a new rate constant, k_{dec}, given by k_{dec}= k_{obs} + k_{esc} that is used to determine the number of interest given by γ_{PV}=k_{obs}/ω. The pulsed valve uptake experiments on $CaCO_3$ showed that there is a modest mass-dependence of the measured uptake γ_{PV} by approximately a factor of three to four. For a dose of about 2.5×10^{15} molecules per pulse we observed an unexpected increase of the uptake γ_{PV} with increasing mass of $CaCO_3$ as reported for steady state experiments in Table 5 and displayed in Fig. 4. The increase of γ_{PV} saturates at large sample mass because the number of layers exceeds the depth of diffusion of gas into the internal voids. For all series of pulses the measurements are identical, within the uncertainty, to those for steady state experiments.

Similar behavior has been observed in a recent study carried out by Seisel et al. (Seisel et al., 2005). In that study uptake experiments of N_2O_5 on Saharan Dust obtained from pulsed and steady state experiments were in good agreement, indicating that the steady state uptake coefficients are not influenced by saturation effects under their experimental conditions.

The good agreement between γ_0 from pulsed valve and continuous flow experiments gives us confidence in the large numerical value which precludes pore diffusion. Real-time diffusion tube experiments showed that the interaction of Ar and N_2 molecules with toluene and black decane soot, respectively, does not differ significantly from the one of a Teflon-coated tube (Alcala, 2002). We take this as an indication that on a time scale of a few seconds the gas does not explore the interstitial space of the sample. However, on a much longer time scale slow diffusional processes will transport N_2O_5 into the bulk. Therefore, γ_{ss} is controlled both by saturation as well as by mass transport.

In order to determine the number of sample layers, the total volume of the powder was calculated from its true density (ρ_t=2.93 g/cm^3) and the mass of the sample spread out across the geometric area of the sample holder. The number of formal layers calculated for an average sample grain diameter of 3.5 μm from the average particle size and the height of the sample is reported in Table 5. The typical grain diameter of 3.5 μm has been obtained from the manufacturer's specifications of the used $CaCO_3$ powder and presumably corresponds to the size of the primary $CaCO_3$ particles. Published electron microscopy (SEM) images suggest a grain size diameter that is larger than 3.5 μm as displayed in Fig. 5, presumably owing to agglomeration of primary particles. Following Fig. 4 we make the assumption that the "break" at 330 mg of $CaCO_3$ in the γ_0 and γ_{PV} curve vs. sample mass corresponds to one effective or "nominal" layer of $CaCO_3$ particles that fully covers the geometric surface A_s of the sample support. A mass of 330 mg corresponds to one nominal layer of 57 μm diameter $CaCO_3$ particles "filling" the geometric surface of the sample holder A_s=19.6 cm^2 using an arrangement of closely-packed spherical particles. Thus, one nominal layer of $CaCO_3$ will contain 330 mg $CaCO_3$ of closely packed spheres of "effective" grain diameter of 57 μm knowing full well that the sample in reality is multidisperse and structurally heterogeneous. The linear mass dependence of γ up to a sample mass of 330 mg displayed in Fig. 4 is a consequence of the fact that γ has been calculated using the full value of A_s in the expression for the collision frequency ω although the sample holder was only partially covered with $CaCO_3$ particles. Had we used the true geometric surface area for samples less than 330 mg in the calculation of γ we would have obtained the constant value

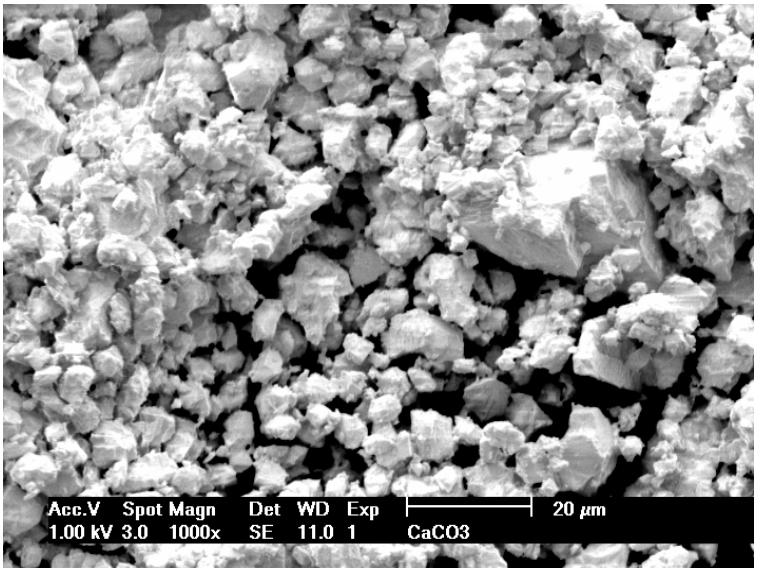

Fig. 5. SEM-image of 5 mg of $CaCO_3$ powder sample used in this work. The dark area is the sample holder.

displayed for sample masses in excess of 330 mg. Therefore, the linear mass dependence is an artifact resulting from the use of a constant value of A_s in the calculation of γ for sample masses corresponding to partial coverage of the sample holder of area A_s with $CaCO_3$ particles of 57 μm diameter.

In contrast, the use of the BET (Brunauer-Emmett-Teller) surface area and the pore diffusion theory (KLM) (Keyser et al., 1991) would substantially underestimate the true uptake coefficient. An alternate interpretation of the same data displayed in Fig. 4 makes use of the assumption that the sample consists of small $CaCO_3$ particles of 3.5 μm diameter leading to a multilayer structure of the sample. This assumption which may be questioned on the basis of the image of the $CaCO_3$ sample displayed in Fig. 5 evidently leads to a multilayer coverage in the linear mass dependence of γ displayed in Fig. 4 in contrast to the partial coverage assumption discussed above. Table 5 reveals that at the "break" point of 330 mg one effective sample layer corresponds to 16 formal layers which is a consequence of the differing particle size, namely 57 vs. 3.5 μm. Owing to the multilayer nature of the sample under this assumption pore diffusion theory has been applied and results in $\gamma_{pd,ss}=(7.4\pm1.7)\times10^{-6}$ using a tortuosity factor τ=2.7 for a grain diameter for $CaCO_3$ of 3.5 μm (dashed curve, Fig. 4). This value of γ is lower by a factor of 10^3 compared to $\gamma_{ss}=(2.8\pm0.5)\times10^{-2}$ and $\gamma_0=0.16\pm0.02$ which were calculated on the basis of the geometrical surface area A_s of the sample as displayed in Table 5. The use of the pore diffusion theory substantially underestimates the true uptake coefficient so that it may be interpreted as a lower limit for γ_g whereas γ_{ss} and γ_0 based on the geometrical surface area may be regarded as an upper limit to the true value of γ.

A supporting argument in favor or using the geometric surface area A_s in evaluating γ comes from pulsed valve experiments whose results are virtually identical to the steady state experiments at "zero" time after the start of the uptake reaction, namely γ_0 (Fig. 1). We support the view that it is improbable for the gas to explore the whole internal (BET) surface area of the sample during a typical pulse decay lasting for a few seconds or so based on diffusion tube experiments under molecular flow conditions performed by Alcala (2002).

In conclusion, we present two main arguments in favor of using the geometric surface area for the calculation of γ pertaining to the interaction of N_2O_5 with $CaCO_3$: (a) the large magnitude of the uptake coefficient, γ_0, γ_{PV}, and γ_{ss} makes diffusion into the interstitial space non-competitive with reaction. This will be even more the case at atmospheric concentrations owing to the observed inverse concentration dependence which has been observed on numerous occasions, for instance for NO_3 free radical interacting with $CaCO_3$ (Karagulian and Rossi, 2005); (b) the good agreement between steady-state and pulsed valve experiments have firmly established the large values of γ_0 which decrease to a steady-state owing to saturation of the uptake. It is thought to be highly unlikely that N_2O_5 is able to explore the internal surface area on the time scale of a pulsed valve uptake experiment. The linear mass dependence of γ from 0 to 330 mg displayed in Fig. 4 is a trivial artifact that is related to the use of A_s in computing γ despite the incomplete coverage of the sample holder with $CaCO_3$ particles.

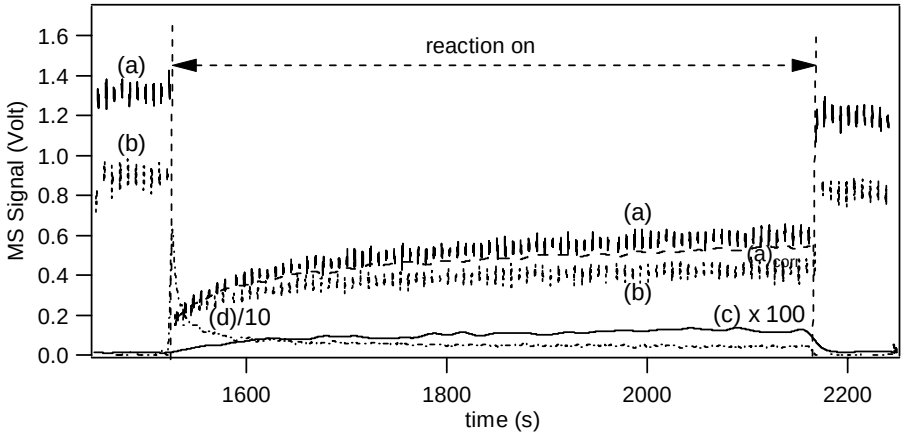

Fig. 6. Typical N_2O_5 uptake experiment on a sample of 1 g of Kaolinite. Curves (a), (b), (c) and (d) correspond to the raw MS signals monitored at m/e 46, m/e 30, m/e 63 and m/e 18, respectively, using an orifice diameter of 8 mm and $[N_2O_5]_0$=(3.8±0.5)×10^{12} cm^{-3}. Curve $(a)_{corr}$ corresponds to the corrected signal at m/e 46 for the presence of HNO_3.

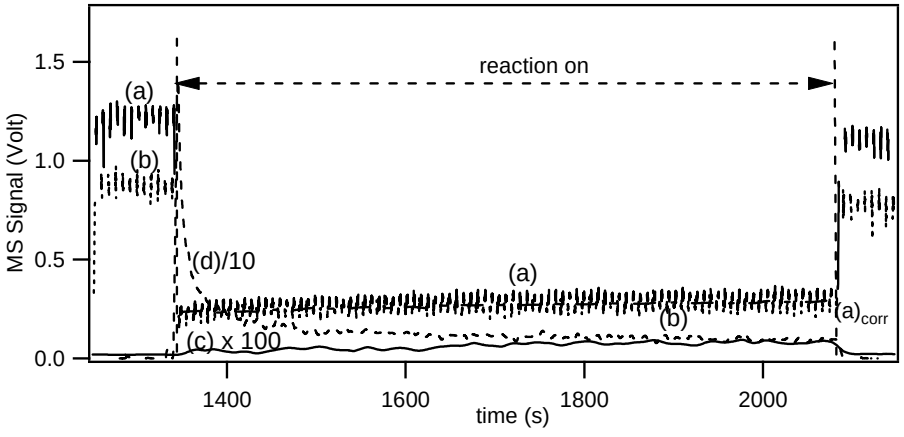

Fig. 7. Typical N_2O_5 uptake experiment on a sample of 1 g of Saharan Dust. Curves (a), (b), (c) and (d) correspond to the raw MS signals monitored at m/e 46, m/e 30, m/e 63 and m/e 18, respectively, using an orifice diameter of 8 mm and $[N_2O_5]_0$=(3.8±0.5)×10^{12} cm^{-3}. Curve $(a)_{corr}$ corresponds to the corrected signal at m/e 46 for the presence of HNO_3.

5 Uptake of N_2O_5 on mineral dust substrates: results and discussion

Table 6 reports results on experiments performed on 1 g samples of surrogate mineral dust powder at a high initial concentration of $[N_2O_5]_0$=(3.8±1.0)×10^{12} cm^{-3}. The steady-state uptake coefficients γ_{ss} of N_2O_5 range from (2.2±0.6)×10^{-3} for natural limestone to (5.9±1.6)×10^{-2} for Saharan Dust using the geometric surface area. At a lower initial concentration of $[N_2O_5]_0$=(4.0±1.0)×10^{11} cm^{-3} uptake experiments performed on 0.3 g have revealed larger values of γ_{ss} ranging from (3.5±1.1)×10^{-2} for $CaCO_3$ to 0.2±0.05 for Saharan Dust. We also report the observed initial uptake coefficients γ_0 for N_2O_5 on all the samples of mineral dust at low and high values of $[N_2O_5]$. For a concentration of $[N_2O_5]_0$=(3.8± 0.5)×10^{12} cm^{-3} the γ_0 values range from (6.4±1.9)×10^{-3} for Arizona test dust to (9.0±2.6)×10^{-2} for Saharan Dust, whereas at $[N_2O_5]_0$=(4.0±1.0)×10^{11} cm^{-3} the γ_0 values range from 0.12±0.04 for $CaCO_3$ to 0.43±0.13 for natural limestone. For samples such as Saharan Dust, $CaCO_3$ and Arizona Test Dust values of γ_{ss} and γ_0 decrease between a factor of 3 and 7 from low to high $[N_2O_5]_0$. As indicated in Table 6, both the values γ_{ss} and γ_0 for $CaCO_3$ decrease only by a factor 3.5 from low to high $[N_2O_5]$. On the other hand, a particular case is represented by natural limestone which showed a decrease of γ_{ss} and γ_0 by a factor of 20 and 40, respectively, when increasing $[N_2O_5]_0$. $CaCO_3$ showed values of γ_{ss} and γ_0 higher by a factor of 3 with respect to natural limestone at high $[N_2O_5]_0$. This difference is reversed by the same amount for low $[N_2O_5]_0$ with γ of natural limestone being highly sensitive to saturation by $[N_2O_5]$. Natural limestone

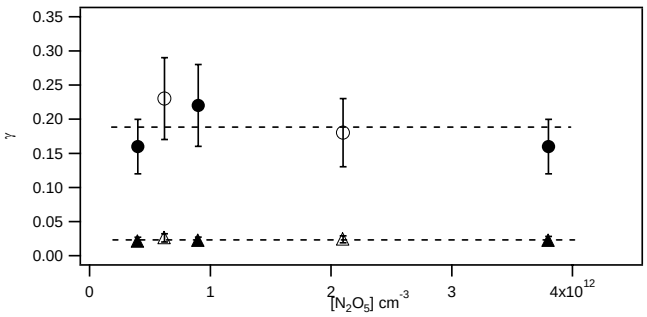

Fig. 8. N_2O_5 on 200 mg Kaolinite: uptake coefficient γ of N_2O_5 as a function of $[N_2O_5]$: initial (γ_0, open circles) and steady state (γ_{ss}, full triangles) uptake coefficients for A_s=4.9 cm^2. Full and empty symbols are referred to uptake experiments carried out with an orifice diameter of 4 and 8 mm orifice diameter, respectively.

is a sedimentary rock containing 97% $CaCO_3$ by weight and a small percentage of metal oxides (see Table 2) that may be responsible for the difference in the kinetic properties of $CaCO_3$ and natural limestone. In recent work Krueger and co-workers (Krueger et al., 2005), showed that dust containing calcium is very reactive with respect to the uptake of nitric acid. However, because of differences in mineralogy of single dust-particles, not all of the calcium-containing particles react similarly.

It is important to note that for Kaolinite γ_{ss} and γ_0 are independent of $[N_2O_5]_0$ over the investigated range. Typical raw data from an uptake experiment of N_2O_5 on 1 g of Kaolinite and Saharan Dust are shown in Figs. 6 and 7. In this series of experiments we did not succeed to saturate the samples during the present observation period. Uptake experiments of N_2O_5 on 0.2 g of Kaolinite powder were carried out by varying the initial flow of N_2O_5 into the reactor (Table 7). Figure 8 displays data for the 8 mm orifice corresponding to a residence time τ_g of 1.32 s for a variation of $[N_2O_5]_0$ by a factor 9.5 that is between $(4.0\pm1.0)\times10^{11}$ cm^{-3} and $(3.8\pm0.5)\times10^{12}$ cm^{-3}. Figure 8 shows that both γ_0 and γ_{ss} remain constant at 0.19±0.05 and $(2.3\pm0.6)\times10^{-2}$, respectively, with increasing $[N_2O_5]$ and by changing the gas residence time τ_g. From this series of measurements it is evident that γ_{ss} follows a pseudo first order rate law in N_2O_5 in contrast to the other substrates which showed a decreasing trend from low to high $[N_2O_5]$ (see Fig. 3 and Table 6).

In recent work the uptake of N_2O_5 on Saharan Dust was found to be independent of $[N_2O_5]$ (Seisel et al., 2005). An initial uptake $\gamma_0=(8.0\pm0.3)\times10^{-2}$ was found, whereas the steady state value $\gamma_{ss}=(1.3\pm0.3)\times10^{-2}$ was lower by a factor of five with respect to the present results at $[N_2O_5]_0=(3.8\pm0.5)\times10^{12}$ cm^{-3} for reasons that are not apparent.

We have observed delayed production of HNO_3 upon uptake of N_2O_5 for every sample investigated. Gas phase HNO_3 formation may be due to the heterogeneous hydrolysis of N_2O_5 according to Reaction (R9). In order to understand the gas phase production of HNO_3 we want to stress that all the investigated samples have a non negligible amount of adsorbed water available on the substrate surface. The quantities of $H_2O_{(ads)}$ that still remain on the different mineral dust substrates at our experimental conditions as reported in Table 6 and were measured by gravimetric measurements. The hygroscopic properties of mineral aerosol samples have been examined in recent work (Gustafsson et al., 2005) which showed significant water adsorption on Arizona Test Dust compared to $CaCO_3$. In Table 6 we also report the percentage of gas phase HNO_3 produced with respect to N_2O_5 taken up during a reaction time of 200 s. At $[N_2O_5]=(3.8\pm0.5)\times10^{12}$ cm^{-3}, Arizona Test Dust and Kaolinite turned out to be the samples to produce the largest amount of gas phase HNO_3, that is 72% and 30%, respectively, with respect to N_2O_5 taken up. On the other hand, Saharan Dust and $CaCO_3$ have been the samples with a lower yield of absolute HNO_3 produced, namely 5% and 6%, respectively. At $[N_2O_5]=(4.0\pm1.0)\times10^{11}$ cm^{-3} we obtained lower yields of gas phase HNO_3 compared to $[N_2O_5]$ ten times higher. In this case we may correlate the low yield of HNO_3 to the large rate of uptake of N_2O_5 and of HNO_3 on mineral dust. Adsorbed HNO_3 may then form salts such as $Ca(NO_3)_2$, $Fe(NO_3)_3$ and surface nitrates as shown in other experimental studies (Börensen et al., 2000; Goodman et al., 2001; Vogt and Finlayson-Pitts, 1994). A recent study on the reactivity of gaseous HNO_3 on atmospheric mineral dust samples reported values for the uptake of HNO_3 on $CaCO_3$, Saharan Dust and Arizona Test Dust (Hanisch and Crowley, 2001a). In that work, a value of γ_0=0.11 based on the geometric surface area was determined for Saharan Dust at $[HNO_3]=(5.6\pm0.4)\times10^{11}$ cm^{-3}, 0.14 for $CaCO_3$ and 6.6×10^{-2} for Arizona Test Dust. These results are consistent with the trend of the present yields of HNO_3 measured for nominally the same mineral dust samples. Whenever the uptake coefficient of HNO_3 on the mineral substrates was low such as for Arizona Test Dust and Kaolinite, we find increased amounts of HNO_3 in the gas phase. Conversely, the reverse is true for samples that rapidly take up HNO_3 as for $CaCO_3$ and Saharan Dust (Börensen et al., 2000).

6 Conclusions and atmospheric implications

We have shown in this work that N_2O_5 undergoes a heterogeneous reaction with surrogate substrates of mineral dust aerosol at T=298±2 K. The measured uptake coefficient showed different values for high and low N_2O_5 concentrations with the least differences for Saharan Dust. These γ values are generally larger than the ones used in a recent global modeling simulation of heterogeneous chemistry on mineral dust aerosol at dry conditions (Bauer et al., 2004) where $\gamma=3.0\times10^{-3}$ for N_2O_5 has been used. The γ values resulting from the present measurements are larger by at least

Table 5. Summary of uptake experiments with N_2O_5 on $CaCO_3$ as a function of sample mass ($[N_2O_5]=(4.0\pm1.0)\times10^{11}\,cm^{-3}$, orifice diameter=14 mm, $A_s=19.6\,cm^2$).

Mass (g)	γ_{ss}	γ_0	$\gamma_{0(pulsed\ valve)}$	[a] Number of formal layers	[b] Number of nominal layers
0.11	$(8.0\pm5.0)\times10^{-3}$	$(5.5\pm2.0)\times10^{-2}$	$(4.7\pm1.5)\times10^{-2}$	5	0.3
0.15	$(1.5\pm0.5)\times10^{-2}$	$(6.4\pm3.0)\times10^{-2}$		7	0.5
0.33	$(2.0\pm0.6)\times10^{-2}$	0.16 ± 0.03	0.13 ± 0.018	16	1
0.51	$(2.2\pm0.5)\times10^{-2}$	0.2 ± 0.02		25	1.5
0.58	$(2.3\pm0.5)\times10^{-2}$	0.18 ± 0.02		30	1.8
0.73	$(2.4\pm0.5)\times10^{-2}$	0.22 ± 0.02	0.21 ± 0.016	36	2.2
1.0	$(2.7\pm0.4)\times10^{-2}$	0.15 ± 0.025		50	3
1.3	$(2.8\pm0.5)\times10^{-2}$	0.16 ± 0.024		64	4
1.6	$(2.8\pm0.5)\times10^{-2}$	0.15 ± 0.024	0.15 ± 0.015	80	5
1.8	$(2.8\pm0.5)\times10^{-2}$	0.17 ± 0.03		90	5.5

Effective diameter of [a] 3.5 μm and [b] 57 μm.

Table 6. Summary of uptake experiments of N_2O_5 on mineral dust samples: initial (γ_0) and steady state (γ_{ss}) uptake coefficients.

Mineral dust sample	[a]γ_0	[a]γ_{ss}	[a]HNO_3	$H_2O_{(ads)}$ [mg g^{-1}]
Kaolinite	0.14 ± 0.04	$(2.2\pm0.6)\times10^{-2}$	30%	23
Natural Limestone	$(1.1\pm0.3)\times10^{-2}$	$(2.2\pm0.6)\times10^{-3}$	18%	7
Arizona Test Dust	$(6.4\pm1.9)\times10^{-2}$	$(1.6\pm0.4)\times10^{-2}$	72%	22
$CaCO_3$	$(3.3\pm1.0)\times10^{-2}$	$(6.2\pm1.8)\times10^{-3}$	5%	4
Saharan Dust	$(9.0\pm2.6)\times10^{-2}$	$(5.9\pm1.6)\times10^{-2}$	6%	20
	[b]γ_0	[b]γ_{ss}	[b]HNO_3	
Kaolinite	(0.16 ± 0.04)	$(2.1\pm0.6)\times10^{-2}$	17%	
Natural Limestone	(0.43 ± 0.13)	$(4.3\pm1.3)\times10^{-2}$	12%	
Arizona Test Dust	(0.2 ± 0.06)	(0.11 ± 0.03)	20%	
CaCO3	(0.12 ± 0.04)	$(2.1\pm0.6)\times10^{-2}$	5%	
Saharan Dust	(0.3 ± 0.08)	0.2 ± 0.05	4%	

Uptake experiments were performed at [a]$[N_2O_5]_0=(3.8\pm0.5)\times10^{12}\,cm^{-3}$ using 1 g of sample powder for $A_s=19.6\,cm^2$; [b]$[N_2O_5]_0=(4.0\pm1.0)\times10^{11}\,cm^{-3}$ using 300 mg of sample powder for $A_s=4.9\,cm^2$. The yield of HNO_3 is given as a percentage with respect to the total molecules of N_2O_5 taken up after a given reaction time of 200 s at orifice diameter of 8 mm.

a factor of 10. Therefore, the uptake of N_2O_5 on mineral dust aerosols may potentially have a greater influence on the reduction of the global ozone concentration compared to the estimated value of 0.7% (Bauer et al., 2004).

In a recent laboratory study on the heterogeneous reaction of N_2O_5 with Saharan dust Seisel et al. (2005) found $\gamma_0=(8.0\pm0.3)\times10^{-2}$ and $\gamma_{ss}=(1.3\pm0.3)\times10^{-2}$, respectively, at $[N_2O_5]=9.0\times10^{10}\,cm^{-3}$. At $[N_2O_5]=(4.0\pm1.0)\times10^{11}\,cm^{-3}$ used in this work (Table 6), we have found values for γ_0 and γ_{ss} larger by a factor of 4 and 15, respectively. In a recent numerical modeling study the interaction of N_2O_5 (γ=0.1), O_3 and HO_2 radicals with dust resulted in a decrease of tropospheric ozone of up to 10% near the dust source areas. (Dentener et al., 1996). In comparison, the measured uptake coefficient γ of N_2O_5 on sulfuric acid aerosols was reported to lie within the range 0.06–0.12 at a temperature between 230 and 300 K (Hanson and Lovejoy, 1994). Other measurements reported γ values of 0.05 on aqueous surfaces over a temperature range from 282 to 294 K (van Doren et al., 1990).

The photolysis rate of NO_3 ($J(NO_3)=0.2\,s^{-1}$) is too fast to allow recombination with NO_2 to N_2O_5 during daylight. Therefore, the heterogeneous chemistry of N_2O_5 is important only at night-time. The heterogeneous reaction of N_2O_5 is most effective during the night when rh is at a maximum in the boundary layer. Thus, under these conditions, dust particles are likely to contain significant quantities of adsorbed water and the assumed high values of γ seem justified (Dentener and Crutzen, 1993). In a recent global modeling study γ=0.02 (rh=70%) and $\gamma=3.0\times10^{-3}$ (rh=30%) for

Table 7. Summary of uptake experiments of N_2O_5 on 200 mg Kaolinite for data plotted in Fig. 8: initial (γ_0) and steady state (γ_{ss}) uptake coefficients (A_s=4.9 cm^2).

$[N_2O_5]$ molecules cm^{-3}	γ_0	γ_{ss}
[a](4.0±1.0)×10^{11}	0.16±0.04	(2.1±0.6)×10^{-2}
[b](6.2±1.5)×10^{11}	0.23±0.06	(2.6±0.5)×10^{-2}
[a](9.0±0.5)×10^{11}	0.22±0.06	(2.2±0.5)×10^{-2}
[b](2.1±0.5)×10^{12}	0.18±0.05	(2.4±0.7)×10^{-2}
[a](3.8±0.5)×10^{12}	0.16±0.04	(2.2±0.6)×10^{-2}

[a] Orifice diameter=8mm; [b] Orifice diameter=4 mm.

humid and dry conditions have been used as upper and lower limits, respectively (Bauer et al., 2004). The modeling results show that when applying the high value for the uptake coefficient 0.8% of the global ozone mass is removed by uptake of N_2O_5 on aerosols. The observed reaction products of the heterogeneous reaction of N_2O_5 with mineral dust, mainly HNO_3, may also have an influence on the oxidizing potential of the atmosphere as well as on the atmospheric ozone balance. Previous laboratory work (Goodman et al., 2000; Hanisch and Crowley, 2001a; Seisel et al., 2004) has shown the importance of the reactivity of HNO_3 on mineral dust substrates. In addition, modeling studies have quantitatively shown decreases in ozone concentration close to the area of HNO_3 destruction (Bauer et al., 2004).

The Saharan dust sample, from Cape Verde (SDCV), that we have used is mineralogically representative of atmospheric dust aerosol. Its composition has been described in the literature (Coudé-gaussen et al., 1994) and closely simulates atmospheric particles of crustal origin (Desboeufs et al., 1999). The clay fraction (<2 μm) of dust from Cape Verde shows a kaolinite-illite-chlorite assemblage which is typical for central Saharan Dust. In the free troposphere mineral dust aerosol of a size less than 2 μm have a settling velocity of approximately 50 cm h^{-1} (Seinfeld and Pandis, 1998). Therefore it can remain in the atmosphere for several days, travel long distances and undergo heterogeneous reactions with trace gases.

The loss rate constant (k_{het}^{M}) due to heterogeneous uptake of a gas species M onto small aerosol particles is given by $k_{\text{het}}^{M}=\gamma A\bar{c}/4$ if the rate is not limited by diffusion, where γ is the uptake coefficient of M and is a function of the mineral dust aerosol composition, A is the surface area density of the dust aerosol and $\bar{c}$ is the mean molecular speed of M. Assuming a surface area density for Saharan Dust of about 1.5×10^{-6} cm^2 cm^{-3} (de Reus et al., 2000), we estimate $k_{\text{het}}^{N_2O_5}=1.76\times10^{-3}$ s^{-1} ($\tau_{\text{het}}^{N_2O_5}$=9.5 min) for N_2O_5 based on γ=0.2 for Saharan dust at $[N_2O_5]<(4.0\pm1.0)\times10^{11}$ cm^{-3} (16 ppb). From the difference between the N_2O_5 formation and loss in the presence of the equilibrium with NO_3 we obtain the expression for the N_2O_5 steady state lifetime given in Eq. (4) (Brown et al., 2003):

$$\tau_{ss}^{N_2O_5}=\left(k_{\text{het}}^{N_2O_5}+\frac{k_{\text{het}}^{NO_3}k_1(T)}{k_{-1}\,[NO_2]}\right)^{-1} \quad (4)$$

$k_1(T)$ and k_{-1} are the rate constant for thermal decomposition of N_2O_5 and its inverse at atmospheric pressure according to equilibrium (R1), respectively. From recent work on the NO_3 heterogeneous reaction on mineral dust we have obtained γ=0.2 which leads to $k_{\text{het}}^{NO_3}=2.4\times10^{-3}$ s^{-1} ($\tau_{\text{het}}^{NO_3}$=7 min) for NO_3 (Karagulian and Rossi, 2005).

At T=273 K $k_1(273K)=3.1\times10^{-3}$ s^{-1}(τ=5 min) (Atkinson et al., 1997) and equilibrium (R1) is shifted to the left. For $[NO_2]$ a typical value is 10 ppb in polluted air so that the pseudo first-order recombination rate constant k_{-1} $[NO_2]$ is 0.48 s^{-1} which is much larger than the rate constant for heterogeneous loss $k_{\text{het}}^{NO_3}=2.4\times10^{-3}$ s^{-1}. Therefore, the second term of Eq. (4) will be negligible and the steady state lifetime $\tau_{\text{ss}}^{N_2O_5}$ of N_2O_5 will be determined by its heterogeneous loss rate constant $k_{\text{het}}^{N_2O_5}$.

At T=293 K equilibrium (R1) is shifted to the right with k_1(293 K)=4.6×10^{-2} s^{-1} (τ=20 s) which is an order of magnitude larger than at T=273 K. Therefore, both terms in Eq. (4) will be of comparable magnitude which will decrease the steady state lifetime of N_2O_5 with respect to 273 K somewhat.

The calculated overall steady state lifetime for N_2O_5 at 293 K ($\tau_{\text{ss}}^{N_2O_5}$=8.5 min) is significantly larger than the thermal dissociation lifetime (τ=20 s) of N_2O_5. At the same surface area concentration for dust aerosol of 1.5×10^{-6} cm^2 cm^{-3}, the heterogeneous loss rate $k_{\text{het}}^{\text{hydr}}$ due to hydrolysis (Reaction R2) is 2.25×10^{-4} s^{-1} corresponding to a lifetime of 74 min. This means that some N_2O_5 may be irreversibly converted to HNO_3 during the night by hydrolysis.

During January 2004, Wood (Wood et al., 2005) performed in situ measurement of N_2O_5 in Contra Costa Country, California, and derived a steady state lifetime for N_2O_5 that ranged from 5 to 30 min at $[N_2O_5]$=200 ppt (5.0×10^9 cm^{-3}) in the temperature range 275–285 K which is comparable to $\tau_{\text{ss}}^{N_2O_5}$ calculated above. With an estimated value of γ=0.07 Wood et al. derived a total estimated aerosol surface area of 200 μm^{-2} cm^{-3} from the above measured N_2O_5 lifetime. The γ_0 value of 0.2 for mineral dust aerosol measured in this work is consistent with the field measurement in the presence of an "urban aerosol" which certainly does not correspond to a typical mineral dust aerosol. Clearly, a quantitative comparison is not possible owing to lack of data. However, with an uptake coefficient lower by three orders of magnitude such as pore diffusion corrected the aerosol loading would have to be higher by the same factor at constant N_2O_5 lifetime which may be excluded on experimental grounds as it is already quite high for a suburban environment. The measured lifetime for N_2O_5 from the field

is thus consistent with the heterogeneous loss rates of NO_3 and N_2O_5 measured in the present work.

Acknowledgements. We gratefully acknowledge OFES for funding this work in the context of the EU subproject MINATROC which is part of the EU Environment and Climate Program.

Edited by: J. N. Crowley

References

Alcala, C.: Heterogeneous reactions of the exhaust gas components nitrogen dioxide and water on flame soot: a molecular diffusion tube study., EPFL (Thesis work), 107–108, 2002.

Al-Hosney, H. A. and Grassian, V. H.: Carbonic acid: An important intermediate in the surface chemistry of calcium carbonate, J. Am. Chem. Soc., 126, 8068–8069, 2004.

Atkinson, R., Baulch, D. L., Cox, R. A., Hampson, R. F., Kerr, J. A., Rossi, M. J., and Troe, J.: Evaluated kinetic and photochemical data for atmospheric chemistry: Supplement VI – IUPAC subcommittee on gas kinetic data evaluation for atmospheric chemistry, J. Phys. Chem. Ref. Data, 26, 1329–1499, 1997.

Bauer, S. E., Balkanski, Y., Schulz, M., Hauglustaine, D. A., and Dentener, F.: Global modeling of heterogeneous chemistry on mineral aerosol surfaces: Influence on tropospheric ozone chemistry and comparison to observations, J. Geophys. Res.-Atmos., 109, D02304, doi:10.1029/2003JD003868., 2004.

Bian, H. S. and Zender, C. S.: Mineral dust and global tropospheric chemistry: Relative roles of photolysis and heterogeneous uptake, J. Geophys. Res.-Atmos., 108, 4672, doi:10.1029/2002JD003143., 2003.

Bonasoni, P., Cristofanelli, P., Calzolari, F., Bonafé, U., Evangelisti, F., Stohl, A., Sajani, S. Z., van Dingenen, R., Colombo, T., and Balkanski, Y.: Aerosol-ozone correlations during dust transport episodes, Atmos. Chem. Phys., 4, 1201–1215, 2004.

Börensen, C., Kirchner, U., Scheer, V., Vogt, R., and Zellner, R.: Mechanism and kinetics of the reactions of NO_2 or HNO_3 with alumina as a mineral dust model compound, J. Phys. Chem. A, 104, 5036–5045, 2000.

Brown, S. S., Stark, H., and Ravishankara, A. R.: Applicability of the steady state approximation to the interpretation of atmospheric observations of NO_2 and N_2O_5, J. Geophys. Res.-Atmos., 108(B3), 2162, doi:10.1029/2002JD002917, 2003.

Buhmann, D. and Dreybrodt, W.: The Kinetics of Calcite Dissolution and Precipitation in Geologically Relevant Situations of Karst Areas .1. Open System, Chem. Geol., 48, 189–211, 1985.

Caloz, F., Fenter, F. F., Tabor, K. D., and Rossi, M. J.: Paper I: Design and construction of a Knudsen cell reactor for the study of heterogeneous reactions over the temperature range 130–750 K: Performances and limitations, Rev. Sci. Instrum., 68, 3172–3179, 1997.

Coudé-gaussen, G., Rognon, P., and Lecoustumer, M.: Gradual Input of Saharan Dust in the Silty Deposits of the Eastern Cape-Verde Islands, Comptes Rendus De L'Académie des Sciences Serie II, 319, 1343–1349, 1994.

De Leeuw, N. H. and Parker, S. C.: Surface structure and morphology of calcium carbonate polymorphs calcite, aragonite, and vaterite: An atomistic approach, J. Phys. Chem. B, 102, 2914–2922, 1998.

de Reus, M., Dentener, F., Thomas, A., Borrmann, S., Strom, J., and Lelieveld, J.: Airborne observations of dust aerosol over the North Atlantic Ocean during ACE 2: Indications for heterogeneous ozone destruction, J. Geophys. Res.-Atmos., 105, 15 263–15 275, 2000.

de Reus, M., Fischer, H., Sander, R., Gros, V., Kormann, R., Salisbury, G., Van Dingenen, R., Williams, J., Zollner, M., and Lelieveld, J.: Observations and model calculations of trace gas scavenging in a dense Saharan dust plume during MINATROC, Atmos. Chem. Phys., 5, 1787–1803, 2005.

Dentener, F. J., Carmichael, G. R., Zhang, Y., Lelieveld, J., and Crutzen, P. J.: Role of mineral aerosol as a reactive surface in the global troposphere, J. Geophys. Res.-Atmos., 101, 22 869–22 889, doi:10.1029/96JD01818., 1996.

Dentener, F. J. and Crutzen, P. J.: Reaction of N_2O_5 on Tropospheric Aerosols - Impact on the Global Distributions of NO_x, O_3, and OH, J. Geophys. Res.-Atmos., 98, 7149–7163, 1993.

Desboeufs, K. V., Losno, R., Vimeux, F., and Cholbi, S.: The pH-dependent dissolution of wind-transported Saharan dust, J. Geophys. Res.-Atmos., 104, 21 287–21 299, 1999.

Dreybrodt, W., Eisenlohr, L., Madry, B., and Ringer, S.: Precipitation kinetics of calcite in the system $CaCO_3$-H_2O-CO_2: The conversion to CO_2 by the slow process H^++HCO_3–>CO_2+H_2O as a rate limiting step, Geochim. Cosmochim. Acta, 61, 3897–3904, 1997.

Dreybrodt, W., Lauckner, J., Liu, Z. H., Svensson, U., and Buhmann, D.: The kinetics of the reaction CO_2+H_2O^-–> H^++HCO_3^- as one of the rate limiting steps for the dissolution of calcite in the system H_2O-CO_2-$CaCO_3$, Geochim. Cosmochim. Acta, 60, 3375–3381, 1996.

Fenter, F. F., Caloz, F., and Rossi, M. J.: Experimental evidence for the Efficient Dry Deposition of Nitric Acid on Calcite, Atmos. Environ., 29, 3365–3372, 1995.

Frinak, E. K., Wermeille, S. J., Mashburn, C. D., Tolbert, M. A., and Pursell, C. J.: Heterogeneous reaction of gaseous nitric acid on gamma-phase iron(III) oxide, J. Phys. Chem. A, 108, 1560–1566, 2004.

Goodman, A. L., Bernard, E. T., and Grassian, V. H.: Spectroscopic study of nitric acid and water adsorption on oxide particles: Enhanced nitric acid uptake kinetics in the presence of adsorbed water, J. Phys. Chem. A, 105, 6443–6457, 2001.

Goodman, A. L., Underwood, G. M., and Grassian, V. H.: A laboratory study of the heterogeneous reaction of nitric acid on calcium carbonate particles, J. Geophys. Res.-Atmos., 105, 29 053–29 064, 2000.

Gustafsson, R. J., Orlov, A., Badger, C. L., Griffiths, P. T., Cox, R. A., and Lambert, R. M.: A comprehnsive evaluation of water uptake on atmospheric relevant mineral survaces: DRIFTS spectroscopy, thermogravinetric analysis and aerosol growth measurements, Atmos. Chem. Phys., 5, 3415–3421, 2005.

Hanisch, F. and Crowley, J. N.: Heterogeneous reactivity of gaseous nitric acid on Al_2O_3, $CaCO_3$, and atmospheric dust samples: A Knudsen cell study, J. Phys. Chem. A, 105, 3096–3106, 2001a.

Hanisch, F. and Crowley, J. N.: The heterogeneous reactivity of gaseous nitric acid on authentic mineral dust samples, and on individual mineral and clay mineral components, Phys. Chem. Chem. Phys., 3, 2474–2482, 2001b.

Hanisch, F. and Crowley, J. N.: Heterogeneous reactivity of NO and HNO_3 on mineral dust in the presence of ozone, Phys. Chem. Chem. Phys., 5, 883–887, 2003c.

Hanisch, F. and Crowley, J. N.: Ozone decomposition on Saharan dust: an experimental investigation, Atmos. Chem. Phys., 3, 119–130, 2003d.

Hanson, D. R. and Lovejoy, E. R.: The Uptake of N_2O_5 onto Small Sulfuric Acid Particles, Geophys. Res. Lett., 21, 2401–2404, 1994.

Hjorth, J., Ottobrini, G., Cappellani, F., and Restelli, G.: A Fourier-Transform Infrared Study of the Rate Constant of the Homogeneous Gas Phase Reaction N_2O_5 + H_2O and Determination of Absolute Infrared Band Intensities of N_2O_5 and HNO_3, J. Phys. Chem., 91, 1565–1568, 1987.

Karagulian, F. and Rossi, M. J.: The heterogeneous chemical kinetics of NO_3 on atmospheric mineral dust surrogates, Phys. Chem. Chem. Phys., 7, 3150–3162, 2005.

Keyser, L. F., Moore, S. B., and Leu, M. T.: Surface-Reaction and Pore Diffusion in Flow Tube Reactors, J. Phys. Chem., 95, 5496–5502, 1991.

Koch, T. G., van den Bergh, H., and Rossi, M. J.: A molecular diffusion tube study of N_2O_5 and $HONO_2$ interacting with NaCl and KBr at ambient temperature, Phys. Chem. Chem. Phys., 1, 2687–2694, 1999.

Krueger, B. J., Grassian, V. H., Cowin, J. P., and Laskin, A.: Heterogeneous chemistry of individual mineral dust particles from different dust source regions: the importance of particle mineralogy (38, 6253, 2004), Atmos. Environ., 39, 395–395, 2005.

Kuriyavar, S. I., Vetrivel, R., Hegde, S. G., Ramaswamy, A. V., Chakrabarty, D., and Mahapatra, S.: Insights into the formation of hydroxyl ions in calcium carbonate: temperature dependent FTIR and molecular modelling studies, J. Mater. Chem., 10, 1835–1840, 2000.

Santschi, C.: Heterogeneous reactions of tropospheric trace-gases on solid model aerosol surface: a laboratory study, EPFL (Thesis work), 254, 2003.

Santschi, C. and Rossi, M. J.: The Uptake of CO_2, SO_2, HNO_3 and HCl on Calcite ($CaCO_3$) at 300 K: mechanism and the role of adsorbed water, J. Phys. Chem., accepted, doi:10.1021/jp056312b , published on web 28 February, 2006.

Seinfeld, J. H. and Pandis, S. P.: Atmospheric Chemistry and Physics, John Wiley & Sons, Inc., 6–8, 1998.

Seisel, S., Börensen, C., Vogt, R., and Zellner, R.: The heterogeneous reaction of HNO_3 on mineral dust and gamma-alumina surfaces: a combined Knudsen cell and DRIFTS study, Phys. Chem. Chem. Phys., 6, 5498–5508, 2004.

Seisel, S., Börensen, C., and Zellner, R.: Kinetics and mechanism of the uptake of N_2O_5 on mineral dust at 298 K, Atmos. Chem. Phys., 5, 3423–3432, 2005.

Stipp, S. L. S., Eggleston, C. M., and Nielsen, B. S.: Calcite Surface structure Observed at Microtopographic and Molecular Scales with Atomic Force Microscopy (AFM), Geochim. Cosmochim. Acta, 58, 3023–3033, 1994.

Tabazadeh, A., Jacobson, M. Z., Singh, H. B., Toon, O. B., Lin, J. S., Chatfield, R. B., Thakur, A. N., Talbot, R. W., and Dibb, J. E.: Nitric acid scavenging by mineral and biomass burning aerosols, Geophys. Res. Lett., 25, 4185–4188, doi:10.1029/1998GL900062, 1998.

Tuazon, E. C., Atkinson, R., Plum, C. N., Winer, A. M., and Pitts, J. N.: The Reaction of Gas Phase N_2O_5 with Water-Vapor, Geophys. Res. Lett., 10, 953–956, 1983.

Underwood, G. M., Li, P., Al-Abadleh, H., and Grassian, V. H.: A Knudsen cell study of the heterogeneous reactivity of nitric acid on oxide and mineral dust particles, J. Phys. Chem. A, 105, 6609–6620, 2001.

Usher, C. R., Michel, A. E., and Grassian, V. H.: Reactions on mineral dust, Chem. Rev., 103, 4883–4939, 2003.

van Doren, J. M., Watson, L. R., Davidovits, P., Worsnop, D. R., Zahniser, M. S., and Kolb, C. E.: Temperature dependence of the Uptake Coefficients of HNO_3, HCl, and N_2O_5 by Water Droplets, J. Phys. Chem., 94, 3265–3269, 1990.

Vogt, R. and Finlayson-Pitts, B. J.: A Diffuse-Reflectance Infrared Fourier-Transform Spectroscopic (Drifts) Study of the Surface reaction of NaCl with Gaseous NO_2 and HNO_3, J. Phys. Chem., 98, 3747–3755, 1994.

Wängberg, I., Etzkorn, T., Barnes, I., Platt, U., and Becker, K. H.: Absolute determination of the temperature behavior of the NO_2+NO_3+(M)<–>N_2O_5+(M) equilibrium, J. Phys. Chem. A, 101, 9694–9698, 1997.

Wood, E. C., Bertram, T. H., Wooldridge, P. J., and Cohen, R. C.: Measurements of N_2O_5, NO_2, and O_3 east of the San Francisco Bay, Atmos. Chem. Phys., 5, 483–491, 2005.

Zhang, Y., Sunwoo, Y., Kotamarthi, V., and Carmichael, R.: Photochemical Oxidant Processes in the Presence of Dust: An Evaluation of the Impact of Dust on Particulate Nitrate and Ozone Formation, J. Appl. Meteorol., 33, 813–824, 1994.